Autotransporters drive biofilm formation and auto-aggregation in the diderm Firmicute Veillonella parvula

Nathalie Bechon, Alicia Jiménez-Fernández, Jerzy Witwinowski, Emilie Bierque, Najwa Taïb, Thomas Cokelaer, Laurence Ma, Jean-Marc Ghigo, Simonetta Gribaldo, Christophe Beloin

Autotransporters drive biofilm formation and auto-aggregation in the diderm Firmicute *Veillonella parvula*.

Nathalie Béchon[1,2,#], Alicia Jiménez-Fernández[1,#], Jerzy Witwinowski[3], Emilie Bierque[1,4,7], Najwa Taib[3,5], Thomas Cokelaer[5,6], Laurence Ma[6], Jean-Marc Ghigo[1], Simonetta Gribaldo[3] and Christophe Beloin[1,*]

[1] Genetics of Biofilm Laboratory, Institut Pasteur, UMR CNRS2001, Paris, 75015, France

[2] Université de Paris, Sorbonne Paris Cité, Paris, France

[3] Unit Evolutionary Biology of the Microbial Cell, Institut Pasteur, UMR CNRS2001, Paris, France

[4] Sorbonne Université, Collège doctoral, F-75005 Paris, France

[5] Hub de Bioinformatique et Biostatistique – Département Biologie Computationnelle, Institut Pasteur, USR 3756 CNRS, Paris, France

[6] Plate-forme Technologique Biomics – Centre de Ressources et Recherches Technologiques (C2RT), Institut Pasteur, Paris, France

[7] Present address: Leptospirosis Research and Expertise Unit, Institut Pasteur in New Caledonia, Institut Pasteur International Network, Noumea, New Caledonia.

[#]The authors equally contributed to the work. Author order was determined alphabetically.

Running Title: Autotransporters drive *V. parvula* biofilm.

***Corresponding author:** Christophe Beloin (christophe.beloin@pasteur.fr)

ABSTRACT

The Negativicutes are a clade of Firmicutes that have retained the ancestral diderm character and possess an outer membrane. One of the best studied Negativicute, *Veillonella parvula*, is an anaerobic commensal and opportunistic pathogen inhabiting complex human microbial communities, including the gut and the dental plaque microbiota. Whereas adhesion and biofilm capacity of *V. parvula* is expected to be crucial for its maintenance and development in these environments, studies of *V. parvula* adhesion have been hindered by the lack of efficient genetic tools to perform functional analyses in this bacterium. Here, we took advantage of a recently described naturally transformable *V. parvula* isolate, SKV38, and adapted tools developed for the closely related *Clostridia spp.* to perform random transposon and targeted mutagenesis to identify *V. parvula* genes involved in biofilm formation. We show that type V secreted autotransporters -typically found in diderm bacteria- are the main determinants of *V. parvula* auto-aggregation and biofilm formation, and compete with each other for binding either to cells or to surfaces, with strong consequences on *V. parvula* biofilm formation capacity. The identified trimeric autotransporters have an original structure compared to classical autotransporters identified in Proteobacteria with an additional C-terminal domain. We also show that inactivation of the gene coding for a poorly characterized metal-dependent phosphohydrolase HD domain protein conserved in the Firmicutes and their closely related diderm phyla inhibits autotransporter-mediated biofilm formation. This study paves the way for further molecular characterization of *V. parvula* interactions with other bacteria and the host within complex microbiota environments.

IMPORTANCE

Veillonella parvula is an anaerobic commensal and opportunistic pathogen whose ability to adhere to surfaces or other bacteria and form biofilms is critical to inhabit complex human microbial communities such as the gut and oral microbiota. Although the adhesive capacity of *V. parvula* has been previously described, very little is known about the underlying molecular mechanisms due to a lack of genetically amenable *Veillonella* strains. In this study, we took advantage of a naturally transformable *V. parvula* isolate and newly adapted genetic tools to identify surface exposed adhesin called autotransporters as the main molecular determinants of adhesion in this bacterium. This work therefore provides new insights on an important aspect of *V. parvula* lifestyle, opening new possibilities for mechanistic studies of the contribution of biofilm formation to the biology of this major commensal of the oral-digestive tract.

INTRODUCTION

Negativicutes are atypical and poorly studied Firmicute lineages displaying an outer envelope with lipopolysaccharide (1). Among the Negativicutes, *Veillonella* spp. are anaerobic diderm cocci that commonly inhabit the human and animal microbiota. One of their best studied species, *Veillonella parvula* (2), is a natural inhabitant of multiple different microbiota, including the human gut (3, 4). *V. parvula* is considered a commensal organism, and proposed to play a role in the development of immunity through its capacity to colonize the infant gut (5, 6). It is a key early colonizer of the dental plaque during the establishment of sessile microbial communities called biofilms (7), promoting multi-species growth and playing a central role in the metabolism of community members through lactic acid consumption (8). However, *V. parvula* is also described as an opportunistic pathogen and has been associated with diverse infections, including osteomyelitis, endocarditis, spondylodiscitis, abscesses as well as systemic infections (9–13).

The importance of *V. parvula* in the development of microbial community spurred our interest in identifying the determinants of its adhesion and biofilm formation capacities. Moreover, considering the presence of an outer membrane in this atypical Firmicute, we wondered whether *V. parvula* uses known diderm or monoderm biofilm determinants, or currently undescribed adhesion factors. We recently studied *V. parvula* DSM2008 as a model diderm Firmicute strain (14) to investigate its outer membrane (OM) protein composition and detected 78 OM proteins, thirteen of which being potential adhesins belonging to the type V family of secreted autotransporter proteins (T5SS) (15). Autotransporter proteins are specifically found in diderms and all share common structural and functional features: a Sec-dependent signal peptide, a passenger domain providing the protein function, and an outer-membrane β-barrel domain that allows secretion of the passenger domain (16). However, the challenge of genetic manipulation in *V. parvula* DSM2008 severely limited the study of these adhesins in this strain.

Here, we have sequenced and annotated the genome of *V. parvula* SKV38, a recently isolated, naturally transformable and genetically amenable strain (17). We adapted and developed genetic tools for this organism, permitting random and site directed mutagenesis, plasmid complementation and controlled expression using an inducible promoter. This enabled us to identify and characterize factors involved in *V. parvula* biofilm formation. We find that the main *V. parvula* biofilm modulating determinants are T5SS adhesins, i.e. typical diderm

89 determinants. Interestingly, the identified adhesins possess an additional C-terminal domain
90 compared to the known domain architecture of classical autotransporters. We also show that a
91 locus encoding a metal-dependent phosphohydrolase HD domain protein is involved in biofilm
92 formation, similarly to what was shown in the prototypical monoderm *Bacillus subtilis* (18).
93 Therefore, our results demonstrate that diderm Firmicutes use a mixture of diderm and
94 monoderm factors to modulate their ability to engage into biofilm lifestyle, supporting the idea
95 that monoderm and diderm molecular systems could have co-evolved in these atypical
96 Firmicutes.

97

RESULTS

Random transposon mutagenesis reveals two *V. parvula* SKV38 genes involved in biofilm formation

In order to obtain a framework for genetic work in the recently described naturally competent *V. parvula* SKV38 isolate, we sequenced it using PacBio technology. We obtained a completely assembled genome of 2.146Mbp, encoding 1,912 predicted protein-encoding open reading frame (ORF), 12 rRNA, 49 tRNA and one tmRNA (see Material and Methods). We performed random transposon mutagenesis in *V. parvula* SKV38 using the pRPF215 plasmid carrying an inducible transposase and a mariner-based transposon previously used to mutagenize *Clostridioides difficile* (19), a close relative of the Negativicutes. We screened 940 individual transposon mutants for biofilm formation using crystal violet staining (CV) static biofilm assay in 96-well microtiter plates and identified eight independent mutants with significant reduction in biofilm formation (Figure 1A). Whole genome sequencing localized the transposons in two loci putatively implicated in biofilm formation (Figure 1B). The most affected mutants correspond to insertions in *FNLLGLLA_00516* (seven mutants), encoding a T5SS type Vc trimeric autotransporter. One transposon mutant was inserted in *FNLLGLLA_01127*, encoding a putative HD phosphatase (Figure 1B).

FNLLGLLA_00516 encodes a trimeric autotransporter involved in auto-aggregation

FNLLGLLA_00516 encodes a protein containing several domains usually identified in the T5SS type Vc trimeric autotransporters. Trimeric autotransporters are OM proteins specific of diderm bacteria that have been widely studied for their ability to bind to different surfaces or to other bacteria (20). *FNLLGLLA_00516* is a homolog of *V. parvula* DSM2008 *vpar_0464*, which encodes a protein that was detected in the OM (15). *FNLLGLLA_00516* was annotated by PROKKA as BtaF, a trimeric autotransporter identified in *Brucella suis* involved in adhesion to extracellular matrix and abiotic surfaces (21). Here, we renamed it *Veillonella* trimeric autotransporter A (VtaA), as the first trimeric autotransporter involved in biofilm formation identified in *V. parvula* SKV38. We deleted the *vtaA* coding sequence and showed that Δ*vtaA* had no growth defect (Figure S1A) but displayed a marked reduction of biofilm formation in 96-well polystyrene microtiter plate (Figure 2A). Moreover, while *V. parvula* SKV38 cultures strongly aggregated, Δ*vtaA* did not (Figure 2B and S2). We constructed the strain *pTet-vtaA*, where the chromosomal *vtaA* gene is placed under the control of a functional tetracycline/anhydrotetracycline (aTc) inducible promoter (Figure S3) and showed that its

aggregation capacity and biofilm formation in 96-well polystyrene microtiter plate directly correlated with aTc concentration (Figure 2C-D), demonstrating that VtaA-mediated cell-to-cell interactions are critical for biofilm formation in these conditions. Whereas the microtiter plate assay corresponds to a static biofilm assay, we also used continuous flow glass microfermentors to investigate the contribution of VtaA to biofilm formation in dynamic conditions. Surprisingly, Δ*vtaA* formed almost six times more biofilm than the WT strain in these conditions (Figure 2E). Accordingly, scanning electronic microscopy (SEM) images of mature biofilms on microscopic plastic slides in microfermentor showed that Δ*vtaA* formed a much thicker biofilm when compared to WT (Figure S4). Altogether, these results suggest that auto-aggregation differentially contributes to biofilm formation in static conditions on hydrophobic surfaces versus continuous flow conditions on hydrophilic surfaces.

V. parvula SKV38 encodes sixteen putative autotransporters in addition to VtaA

The strong biofilm phenotype displayed by the Δ*vtaA* mutant in microfermentor led us to suspect that additional adhesins could modulate *V. parvula* biofilm formation capacity. Indeed, searching the *V. parvula* SKV38 genome revealed multiple genes encoding autotransporters (Table 1): three Va classical monomeric autotransporters with a characteristic PFAM_PF03797 autotransporter ß-domain (renamed *Veillonella* monomeric autotransporter A to C : VmaA to C), and eight other putative Vc trimeric autotransporters with a characteristic PFAM_PF03895 YadA _anchor_domain (renamed *Veillonella* trimeric autotransporter B to I: VtaB to I). We also identified several partial autotransporters: *FNLLGLLA_00035*, that only contains a PFAM_PF11924 Ve inverse autotransporter ß-domain but no putative α-domain that normally carries the function of the protein, and *FNLLGLLA_00036-37* and *FNLLGLLA_00040-41*, which are homologs of *V. parvula* DSM2008 *Vpar_0041* and *Vpar_0048*, respectively, and that appear to be split in SKV38 (Table 1). Interestingly, domain analysis of all trimeric ATs of *V. parvula* SKV38 showed that they possess an extra C-terminal-domain (SLH or coiled-coil domain) after the YadA anchor domain that is not found in classical trimeric ATs. Among those, six autotransporters plus *FNLLGLLA_00035*, *FNLLGLLA_00036-37* and *FNLLGLLA_00040-41* form a potential genomic cluster coding for adhesins (Figure 3A), whereas the six others are located in different areas of the genome (Figure 3B).

We selected eight *Veillonella* strains to study more precisely the evolution of the adhesin cluster, including SKV38 and DSM2008. The trimeric autotransporter adhesins seem to evolve dynamically with numerous domain swaps, duplications and reductions of gene copies, likely

through homologous recombination suggesting rapid evolutionary changes in the repertoire of *Veillonella* adhesins (Figure 4). Duplications and deletions could be eased by the presence of short ORFs annotated as hypothetical proteins presenting a high degree of sequence identity. The most basal strain in the *Veillonella* phylogeny has a minimal cluster of only three adhesins genes. Throughout the *Veillonella* genus, the size of the cluster is very variable with a minimal form in *V. atypica,* with only two adhesins. This specific adhesin locus, immediately upstream of rRNA coding genes, is to our knowledge a peculiar genomic character of the *Veillonella* genus and is not found in other genera of the Veillonellaceae, suggesting it originated in the common ancestor of all *Veillonella* species.

The cluster of trimeric autotransporters is involved in surface binding and not aggregation.

To assess the function of the potential adhesins identified in the *V. parvula* SKV38 genome, we constructed -within the cluster of adhesin genes- independent deletion mutants for the two first autotransporters (*vmaA* and *vtaB*) and a large deletion for the eight adjacent genes encoding trimeric autotransporters or partial trimeric autotransporters, hereafter called Δ*8* *(*Δ*FNLLGLLA_00036* to *vtaF*). We also generated independent individual mutants for each of the six additional autotransporters located outside of the cluster. These mutants were all tested for biofilm formation in 96-well polystyrene plate and aggregation capacities. None of the mutants, with the exception of the previously mentioned Δ*vtaA* strain, was affected for aggregation capacities (Figure 5A). The Δ*8* mutant was the sole mutant, in addition to the Δ*vtaA* mutant, to display lower biofilm formation in 96-well polystyrene microtiter plate (Figure 5B and C), suggesting that the adhesins of this cluster could be involved in biofilm formation independently of cell-to-cell interactions. When tested in microfermentor, Δ*8* displayed a slightly reduced ability to form mature biofilm, however, not statistically different from WT (Figure 5D). This reduced ability to form mature biofilms was actually more visible when observing SEM images, since the Δ*8* mutant only poorly covered the coverslip with sporadic aggregates of cells producing extracellular matrix (Figure S4). Initial adhesion assay to glass spatula showed that both Δ*vtaA* and Δ*8* displayed a lower percentage of initial adhesion than WT, suggesting that VtaA-mediated auto-aggregation contributed to initial adhesion of the WT strain while the adhesin cluster is probably directly involved in surface binding (Figure 5E). This also indicates that Δ*vtaA* does not adhere to glass better than WT, and so the increased biofilm formation of Δ*vta* in microfermenter arises during the continuous flow culture step. The

effect of deleting *vtaA* and the 8 adhesin genes on initial adhesion was additive since a Δ*vtaA*Δ*8* double mutant showed a reduced initial adhesion on microfermentor spatula compared to either WT, Δ*vtaA* or Δ*8* (Figure 5E). In addition, Δ*vtaA*Δ*8* formed 17 times less biofilm than Δ*vtaA* in microfermentor, indicating that in the absence of VtaA, the adhesins encoded by some of these eight genes strongly promote mature biofilm formation in microfermentor (Figure 5D).

Taken together, these results demonstrate the differential contribution of VtaA and part of the cluster of adhesin to *V. parvula* SKV38 adhesion and highlight the existence of potential interference mechanisms between them.

FNLLGLLA_01127 encodes an HD phosphatase that inhibits biofilm formation

In addition to genes encoding potential T5SS proteins, we also identified a transposon mutant in *FNLLGLLA_01127*, encoding a protein of the HD phosphatase superfamily (Figure 1B). The *FNLLGLLA_01127* gene is homologous to YqeK, a putative phosphatase required for pellicle formation and the development of biofilm in *B. subtilis* (18). *FNLLGLLA_01127/yqeK* is found in a cluster of genes (*obg*, *yhbY*, *proB*, *proA*, *nadD*, *yqeK*, *lytR*, and *rsfS*), whose synteny is very well conserved among Negativicutes. This cluster, or part of it, is also well conserved in almost all Firmicutes genomes we analyzed, both monoderm and diderm, as well as in members of other diderm phyla phylogenetically close to the Firmicutes, notably Deinococcus-Thermus (Figure 6 and S5, DataSet 2). A *FNLLGLLA_01127* deletion mutant (Δ*1127*) had a lower carrying capacity compared to WT, maybe due to higher mortality during the stationary phase (Figure S1) and a moderate 1.5-fold decrease in biofilm formation in microtiter plate after correcting for the growth defect (Figure 7A). This mutant also displayed a slightly faster aggregation rate than the WT during early time points (Figure 7B). The strongest phenotype of this mutant was detected in microfermentor with a 9-fold increase in biofilm formation compared to WT (Figure 7C). Expression of *FNLLGLLA_01127* gene *in trans* (plasmid *p1127*) did not complement the observed growth defect (Figure S1B) but it did complement the increased biofilm formation in microfermentor (Figure 7D), showing that deletion of *FNLLGLLA_01127* might have had polar effects on downstream genes of the operon causing a growth defect, but that *FNLLGLLA_01127* alone was responsible for the observed inhibition of biofilm formation. Scanning electronic microscopy showed that Δ*1127*, similarly to Δ*vtaA*, formed a thick layered biofilm, although with fewer filaments and protein deposits compared to WT (Figure 7E). However, contrary to Δ*vtaA* or Δ*8* mutants, Δ*1127* showed no defect in initial adhesion to a glass spatula (Figure 7F). Interestingly, a Δ*1127*Δ*8* double mutant

formed almost 20 times less biofilm than Δ*1127* in microfermentor (Figure 7C), suggesting that at least some of the autotransporters of the cluster were necessary for Δ*1127* observed strong biofilm formation in microfermentor.

235

236 **DISCUSSION**
237

238 Originally described as a social organism mostly living in biofilm communities (8), *Veillonella*
239 is a known bacterial member of multiple human microbiota. Biofilm formation and adhesion
240 are important in these niches, but their study in *Veillonella* has been hindered by the lack of
241 efficient genetic tools. Here, we used genetics tools adapted from *Clostridia* to characterize
242 factors promoting biofilm formation in a naturally competent *Veillonella parvula* isolate.

243 We identified a T5SS type Vc trimeric autotransporter, FNLLGLLA_0516 (VtaA), as an
244 important biofilm factor promoting *V. parvula* SKV38 auto-aggregation. In addition to Hag1,
245 a YadA-like autotransporter identified from the related species *V. atypica* involved in
246 interspecies interactions (22), VtaA represents the second *Veillonella* protein described which
247 is involved in adhesion, and the first involved in abiotic surface adhesion and auto-aggregation
248 in diderm Firmicutes. Beyond the potential impact on *Veillonella* niche colonization,
249 aggregation capacity is known to contribute to bacterial protection from environmental stresses
250 or host responses (23), promotion of host colonization (24), or pathogenesis (25) in various
251 bacterial species. VtaA is homologous to *Brucella suis* trimeric autotransporter BtaF. However,
252 while *B. suis* BtaF promotes biofilm formation *in vitro*, it was not shown to promote aggregation
253 (21), suggesting that these two proteins have different functions.

254 In diderm bacteria such as *E. coli*, self-associating autotransporters (SAATs) from the type Va
255 family and type Vc trimeric autotransporters were shown to contribute to biofilm formation
256 through their self-recognition properties (26–32). However, in *V. parvula* VtaA-mediated auto-
257 aggregation either promoted (plastic surface and static conditions) or strongly impaired (glass
258 surface and continuous-flow conditions) biofilm formation depending on the model used. Δ*vtaA*
259 initially adhered less to glass spatula compared to WT, even though later on it formed much
260 more biofilm, thus we suspect that the material (glass vs. plastic) is not responsible for the
261 observed difference between our two systems. We hypothesize instead that in the WT, VtaA-
262 mediated aggregates are more sensitive to flow than individual cells, and are thus washed out
263 faster of the microfermentor, and that adhesion to surfaces or to the biofilm extracellular matrix
264 is more important than cell-to-cell interactions when the culture is performed under continuous
265 flow.

266 Interference between cell surface structures is a well-described mechanism by which bacteria
267 modulate their adhesion properties. In *E. coli*, multiple structures, such as chaperone-usher

fimbriae, LPS O-antigen or capsules, interfere with the self-recognizing autotransporter Ag43 though unknown mechanisms (33–36). Therefore, it is possible that in *V. parvula*, VtaA could compete with other adhesins through steric hindrance or competition for membrane export and thus limit biofilm formation under continuous-flow conditions. Consistently, Δ*vtaA* enhanced biofilm formation in microfermentor was dependent on the presence of eight genes of the cluster of trimeric autotransporters, suggesting a competition between VtaA and adhesin(s) of this cluster. Moreover, we noticed that both VtaA and the 8-gene cluster are necessary for full initial adhesion to glass spatula in an independent manner, suggesting that any competition between them only arises later on, during continuous-flow cultures. The exact contribution of these different trimeric autotransporters to biofilm formation and their interplay with VtaA will require further characterization.

Analysis of *V. parvula* SKV38 genome revealed the presence of seven other potential full-length autotransporters, but no other types of classical diderm adhesins. None of them appeared to be involved in cell-to-cell interactions or biofilm formation on abiotic surfaces, and their function remains to be fully elucidated. As *V. parvula* is present in different microbiota, it is expected that a large arsenal of adhesion factors is necessary to adhere under different mechanical constraints and on different surfaces, such as tooth enamel or various epithelia. Moreover, *Veillonella* is known to co-aggregate with *Streptococci* (37–39), that produce *Veillonella* favored carbon source, lactate (40), and they were shown to specifically co-aggregate with *Streptococci* and *Actinomyces* strains from the same microbiota, showing that co-aggregation could have strong implication in niche colonization of these bacteria (41). *V. parvula* and other *Veillonella* are also associated to different opportunistic infections and the contribution of their adhesins to pathogenicity remains to be addressed. Finally, some autotransporters have been shown to carry non-adhesive functions, including protease activity (42), but we detected no classical protease domain in the *Veillonella* autotransporters.

Trimeric autotransporters possess a characteristic YadA_anchor domain (PF03895) that is found mainly in Proteobacteria, but also in Cyanobacteria, Verrumicrobia, Planctomycetes, Kiritimatiellaeota, Chlorobi, Synergistetes, Fusobacteria and Negativicutes (https://pfam.xfam.org/family/PF03895, Dec 2019 (43)). Interestingly, the YadA_anchor of *V. parvula* SKV38 and all *Veillonella* trimeric autotransporters is not at the very end of the C-terminus, where it is usually found in Proteobacteria, but is pre-C-terminal, followed by either a coiled domain or a S-layer homology (SLH) domain (Figure 3, DataSet 1). While the function

of the coiled domain is unknown, in some bacteria the periplasmic SLH domain binds to peptidoglycan (44), suggesting that *Veillonella* trimeric autotransporters could be non-covalently attached to the peptidoglycan. These extra-domains after the YadA_anchor are also found in other Negativicutes (notably the extra SLH domain) and in some other diderm phyla phylogenetically related to the Firmicutes such as Synergistetes and Fusobacteria (DataSet 1). In addition to possessing trimeric autotransporters with an extra coiled C-terminus domain, the Fusobacterium *Streptobacillus moniliformis* ATCC14647 carries eight genes encoding unique trimeric autotransporters with an extra OmpA_family domain (PF00691) at their extreme C-terminus, a domain known to display affinity to peptidoglycan (45) (DataSet 1). These data suggest that a subset of phylogenetically close diderm bacteria have evolved trimeric autotransporters integrating different peptidoglycan binding domains. Whether these domains have an impact on trimeric autotransporters function or exposure to the surface, or more generally on outer membrane stabilization is presently unknown.

Our screening also led to the identification of FNLLGLLA_01127, the homolog of *B. subtilis* YqeK, a putative phosphatase required for pellicle formation and the development of biofilm (18). *Staphylococcus aureus* YqeK was recently shown to be a nucleosidase hydrolyzing diadenosine-tetraphosphate (Ap4A) into ADP (46). In *Pseudomonas fluorescens*, an increased level of Ap4A increases cyclic-di-GMP concentration and enhances cell-surface exposure of a large adhesin LapA, thus inducing biofilm formation (47). c-di-GMP regulates biofilm formation by modulating production of a variety cell-surface appendages or exopolysaccharides in both monoderm and diderm bacteria (48–52). Interestingly, *B. subtilis* YqeK induces the *epsA-O* operon, involved in the production of biofilm matrix-forming polysaccharides (53). Deletion of *V. parvula FNLLGLLA_01127* only led to a minor decrease in biofilm formation in 96-well plate, but to a strong increase in continuous-flow biofilm formation that was dependent on the presence of the cluster of trimeric autotransporters. Further work is needed to determine whether FNLLGLLA_01127 directly impacts production of the adhesins of the cluster or participates to the production/regulation of an unknown exopolysaccharide, which, contrary to *B. subtilis*, would interfere with the function or exposure of the adhesins of the cluster rather than favor community development.

In this study we have shown that classical diderm trimeric autotransporters and a potential nucleotidase, conserved both in monoderms and diderms are crucial for adhesion both between cells and/or to surfaces in the diderm Firmicute *V. parvula*. Our work also underscores the rapid

evolution of a diverse arsenal of trimeric autotransporters in the *Veillonella* genus, both in numbers and size, probably by efficient recombination favored by gene clustering, allowing rapid adaptation to changing environments. Taken together, our results suggest a complex interplay at the surface of *V. parvula* between different cell surface structures that may have co-evolved for a long time in these atypical Firmicutes. Much remains to be discovered on the regulatory circuits controlling these adhesion factors and their role in diderm Firmicutes biology.

MATERIALS AND METHODS

Genome preparation and sequencing

V. parvula SKV38 genomic DNA was extracted using Qiagen genomic tip 20G kit. It was sequenced to 1,500X coverage using PacBio sequencing of one single molecule real time (SMRT) cell with no multiplexing using the V2.1 chemistry. Only one SMRT cell was used but with no multiplexing, leading to an unusually large amount of subreads: 3 Gbp, meaning about 1,500X coverage assuming a 2.1 Mbp genome. This yielded 338,310 reads with a mean subread length of 9,080 bp and N50 read length of 13,500 bp. The longest subread length is above 70 kbp. We randomly subsampled the data to avoid misassemblies keeping only 100,000 subreads, which resulted in a 430X coverage. The genome was then assembled using Canu version 1.8 (54) keeping the default parameters. In particular, subread below 1,000 bp were dropped. The error correction steps of the Canu algorithm were not tuned, keeping the parameters that control alignment seed length, read length, overlap length and error rates to their default values. We obtained one contig of 2.146 Mbp and an additional contig of only 1,972 bp that was abandoned due to lack of supporting data and was removed by the circularization process. The obtained assembled genome closely matched the genome size (2.1422 Mbp) and GC content (38.7%, expected 38.6%) of the reference *V. parvula* DSM2008 strain. The resulting assembled genome was polished using Pilon (55) but no correction was required. No gaps or drops of coverage was detected based on sequana_coverage output (56, 57). The completeness of the candidate assembly was assessed to be 98% using the bacteria mode and the bacteria_db9 lineage-specific profile library of BUSCO software (58), while the number of complete duplicated or fragmented BUSCOs remains at 0, indicative of complete assembly. Alignment of all reads show that only 4% (13,028) remained unmapped and 80% of their length were below 2 kbp. The remaining reads (2000 reads) map on various species and could not be further assembled. Overall, these analyses indicate that the final genome assembly is complete and of good quality.

Bioinformatic analyses

The *V. parvula* SKV38 genome was annotated using PROKKA (59). The SKV38 annotated genome sequence was deposited in the ENA (European Nucleotide Archive) under the accession number ERZ1303164.

373 For protein domain visualization, PFAM domains (pfam.xfam.org, Pfam 32.0. (43)) were
374 detected using HMMER (60). Domains with an e-value lower than 10^{-3} were kept and, in case
375 of overlapping domains, the domain having the best e-value was kept. Presence of C-terminal
376 coils structure was determined using the COILS program (https://embnet.vital-
377 it.ch/software/COILS_form.html) (61).

378 The search for HD phosphatase (YqeK) cluster homologs was conducted as follows: a local
379 databank containing 390 genomes representative of bacterial diversity was mined for the
380 presence of a phosphatase containing HD domain (PF01966) using HMMSEARCH and the --
381 cut_ga option. Protein sequences were then filtered using alignment, functional annotation,
382 protein domains presence and phylogeny. Synteny was investigated in the locus around *yqeK*
383 by looking, using MacSyFinder (62), for the presence of at least one of the 7 genes surrounding
384 *yqeK* in *V parvula* SKV38, namely *obg* (containing GTP1_OBG domain, PF01018), *yhbY*
385 (containing CRS1_YhbY domain, PF01985), *proB* (containing AA_kinase domain, PF00696),
386 *proA* (containing Aldedh domain, PF00171), *nadD* (containing CTP_transf_like domain,
387 PF01467), *lytR* (containing LytR_cpsA_psr domain, PF03816) and *rsfS* (containing RsfS
388 domain, PF02410), with no more than eight other genes separating them. All HMM profiles
389 were downloaded from the PFAM site (pfam.xfam.org). As YqeK homologs are widespread in
390 the Firmicutes, another local databank containing 230 representative Firmicutes genomes was
391 queried by the MacSyFinder approach as described above. All trees were visualized with ITOL
392 (63). Details of the results are presented in Dataset S2.

393

394 **Strains and growth conditions**

395 Bacterial strains and plasmids are listed in Table 2. *V. parvula* was grown in either Brain Heart
396 infusion medium (Bacto Brain Heart infusion, Difco) supplemented with 0.1 % L-cysteine and
397 0.6 % sodium DL-lactate (BHILC) or SK medium (10 g L^{-1} tryptone (Difco), 10 g L^{-1} yeast
398 extract (Difco), 0.4 g L^{-1} disodium phosphate, 2 g L^{-1} sodium chloride, and 10 mL L^{-1} 60 %
399 w/v sodium DL-lactate, described in (17)) and incubated at 37°C in anaerobic conditions in
400 anaerobic bags (GENbag anaero, Biomerieux, ref. 45534) or in a C400M Ruskinn anaerobic-
401 microaerophilic station. *Escherichia coli* was grown in Lysogeny Broth (LB) (Corning)
402 medium under aerobic conditions at 37°C. 20 mg L^{-1} chloramphenicol (Cm), 200 mg L^{-1}
403 erythromycin (Ery) or 2.5 mg L^{-1} tetracycline (Tc) were added to *V. parvula* cultures, 100 mg
404 L^{-1} carbenicillin (Cb) or 5 mg L^{-1} tetracycline (Tc) were added to *E. coli* cultures when needed.

100 µg L^{-1} anhydrotetracycline (aTc) was added to induce the pTet promoter unless stated otherwise. All chemicals were purchased from Sigma-Aldrich unless stated otherwise.

Natural transformation

Cells were resuspended in 1 mL SK media adjusted to 0.4-0.8 OD_{600} and 10 µL were dotted on SK-agar petri dishes. On each drop, 0.5-1 µg plasmid or 75-200 ng $µL^{-1}$ linear dsDNA PCR product was added, or water for the negative control. The plates were incubated 48 hours. The biomass was resuspended in 500 µL SK medium and plated on SK-agar supplemented with the corresponding antibiotic and incubated for another 48 hours. Colonies were streaked on fresh selective plates and the correct integration of the construct was confirmed by PCR and sequencing.

Random mariner transposon mutagenesis

Plasmid pRPF215, described for *Clostridium* mutagenesis (Addgene 106377) (19) was transformed into *V. parvula* SKV38 by natural transformation and selected on Cm supplemented SK-agar medium. An overnight culture of *V. parvula* SKV38-pRPF215 in BHILC was then diluted to 0.1 OD_{600} in the same media, supplemented with aTc and grown 5 hours to induce the transposase. After induction, the culture was diluted and plated on BHILC supplemented with Ery and aTc for selection and incubated for 48 hours. From the resulting colonies, 940 were inoculated in Greiner Bio-one polystyrene flat-bottom 96-well plates (655101) and grown in BHILC supplemented with either Ery and aTc, or Cm, to confirm both the presence of the transposon and the loss of pRPF215 and then kept in 15 % glycerol at -80°C. Selected transposon mutants were grown overnight and the genomic DNA was harvested using DNeasy blood and tissue kit (Qiagen). The genomic DNA was then sent for whole genome sequencing at the Mutualized platform for Microbiology of Institut Pasteur.

Cloning-independent allelic exchange mutagenesis

Site-directed mutagenesis of *V. parvula* SK38 strain was performed as described by Knapp and colleagues (17). Briefly, 1-Kb regions upstream and downstream the target sequence and *V. atypica* tetracycline resistance cassette (*tetM* in pBSJL2) or catP resistance cassette from *C. difficile* (catP in pRPF185, Addgene 106367, from (64)) were PCR-amplified with overlapping

primers using Phusion Flash High-Fidelity PCR Master-Mix (Thermo Scientific, F548). PCR products were used as templates in a second PCR round using only the external primers that generated a linear dsDNA with the tetracycline resistance cassette flanked by the upstream and downstream sequences. This construct was transformed into *V. parvula* by natural transformation and its integration into the genome was selected by plating on Tc or Cm supplemented medium. Positive candidates were further confirmed by a set of PCRs and sequencing around the site. Primers used in this study are listed in Table S1.

Complementation

We replaced the tetracycline resistance gene and its *gyrA* promoter of the shuttle vector pBSJL2 by a chloramphenicol resistance gene, P_{cat}:cat from pRPF185 by Gibson assembly. Briefly, the inserts and the plasmids were PCR amplified and then mixed with Gibson master mix 2x (100µL 5X ISO Buffer, 0.2 µL 10,000 U/mL T5 exonuclease (NEB #M0363S), 6.25 µL 2,000 U/mL Phusion HF polymerase (NEB #M0530S), 50 µL 40,000 U/mL Taq DNA ligase (NEB #M0208S), 87 µL dH2O for 24 reactions) and incubated at 50°C for 30-60 min.

The resulting plasmid pBSJL2-cat was digested by Fastdigest *Bam*HI (Thermo scientific) and the band obtained was purified from agarose gel using QIAquick gel extraction kit (Qiagen) to be used as linear plasmid in a second Gibson assembly. The genes and the P_{mdh} promoter of *V. parvula* SKV38 were amplified by PCR using PhusionFlash Master-mix and cloned in pBSJL2-cat using Gibson assembly. The mix was then transformed in *E. coli* DH5α and plated on LB with carbenicillin. The plasmid was harvested by miniprep using QIAprep spin miniprep kit (Qiagen) and transformed in *V. parvula* as described above.

Alternatively, the anhydrotetracycline inducible expression cassette of pRPF185, hereafter referred to as *pTet*, (Addgene 106367, (64)) was inserted along with a chloramphenicol marker right before the ATG of the target gene, following the procedure described above for cloning-independent allelic exchange mutagenesis. The functionality of *pTet* in *V. parvula* was previously verified using measurement of the aTc dependent ß-glucuronidase activity generated by the presence of pRPF185 transformed in *V. parvula* SKV38 (Figure S3).

Biofilm formation in 96-well microtiter plates

Overnight cultures in BHILC medium were diluted to 0.05 OD_{600} and transferred to three Greiner Bio-one polystyrene flat bottom 96-well plates adding 150 µL per well. After 24 hours of static incubation, one of the three plates was resuspended by pipetting to measure OD_{600}

using a TECAN Infinite-M200-Pro spectrophotometer. The two other plates were used for coloration: cultures were removed by pipetting carefully the supernatant out and biofilms fixed with 150 µL Bouin solution (HT10132, Sigma-Aldrich) for 15 minutes. Bouin solution was removed by inversion and the biofilms were washed once in water. The biofilms were stained with 150 µL crystal violet 1 % (V5265, Sigma-Aldrich) for 15 minutes without shaking, then washed in water twice and left to dry. All washes were made by flicking of the plate. After drying the plate, crystal violet was dissolved with 200 µL absolute ethanol and transferred to a clean 96-well plate for OD_{620} measurement (TECAN Infinite-M200-Pro spectrophotometer).

Biofilm formation in microfermentor

Continuous flow non-bubbled microfermentor containing a removable spatula were used as described in (65, 66) (see https://research.pasteur.fr/en/tool/biofilm-microfermenters/). Briefly, a glass spatula was dipped in an overnight culture diluted to 0.5 OD_{600} in 15 mL BHILC for 15 minutes and returned to the fermentor. Biofilm was grown on the spatula for 48 hours at 37°C. BHILC was constantly supplied through a peristaltic pump at 4 rpm. During the last hour, the speed was increased to 10 rpm to remove planktonic bacteria. A mix of filtered 90% nitrogen/5% hydrogen/5% carbon dioxide was also constantly supplied to maintain anaerobic condition. After 48 hours of growth, the spatula was removed, and the biofilm was resuspended by vortexing in 15 mL BHILC. We measured OD_{600} of the resuspended biofilms with Smart Spec Plus spectrophotometer (BioRad).

Aggregation curve

Overnight cultures were diluted to 0.8 OD_{600} in Brain-heart infusion (BHI) media in semi-micro spectrophotometry cuvette (Fisherbrand) and left to sediment on the bench in presence of oxygen, so no growth should occur. OD_{600} was measured every hour in a single point of the cuvette using SmartSpec spectrophotometer (BioRad).

Initial adhesion on glass

Glass spatula from microfermentor (described above) were dipped in overnight cultures diluted to 0.5 OD_{600} in 15 mL Brain-Heart Infusion (BHI) media for 30 minutes to let bacteria adhere. The spatulas were washed once in 15 mL BHI by submersion and the adhering bacteria were resuspended in 15 mL clean BHI by vortexing. The culture used for inoculation, as well as the resuspended bacteria were serially diluted and plated on SK-agar plate for colony forming unit (CFU) counting.

503

504 **Statistical analysis**

505 Statistical analysis was performed using either R and Rstudio software or GraphPad Prism8
506 (GraphPad software, Inc.). We used only non-parametric test, and when applicable corrected
507 for multiple testing. For microfermentor experiments, 4 replicates of each condition were used.
508 For all the other experiments, at least 6 biological replicates in at least 2 independent experiment
509 were used. A cut-off of p-value of 5% was used for all tests. * $p<0.05$; ** $p<0.05$; *** $p<0.005$.
510 For growth curve analyses, we computed the growth rate and carrying capacity of each
511 biological replicates using Growthcurver 0.3.0 package in R and we performed a Mann-
512 Whitney test comparing both parameters for each mutant to the corresponding WT.

513

COMPETING FINANCIAL INTERESTS

The authors declare no competing financial interests.

ACKNOWLEDGEMENTS

We thank Justin Merritt for providing *V. parvula* SKV38 strain, Bruno Dupuy and Robert P. Fagan for providing the different *Clostridium* plasmids, Pierre Simon Garcia for help with the Figure 3 preparation, Daniela Megrian Nuñez and Panagiotis Adam for the genome databank preparation and the platforms France Génomique and IBISA. We wish to acknowledge funding from the French National Research Agency (ANR) (Fir-OM ANR-16-CE12-0010), from the Institut Pasteur “Programmes Transversaux de Recherche” (PTR 39-16), from the French government's Investissement d'Avenir Program, Laboratoire d'Excellence "Integrative Biology of Emerging Infectious Diseases" (grant n°ANR-10-LABX-62-IBEID) and from the Fondation pour la Recherche Médicale (grant DEQ20180339185). N.B. was supported by a MENESR (Ministère Français de l’Education Nationale, de l’Enseignement Supérieur et de la Recherche) fellowship. A.J.F. was supported by a PRESTIGE program from Campus France.

AUTHORS CONTRIBUTIONS

C.B., N.B. and A.J.F. designed the experiments. N.B., A.J.F., E.B. and L.M. performed the experiments. J.W., N.T., and T.C. carried out all genomics and phylogeny analyses under the supervision of SG. N.B., C.B. and A.J.F. wrote the paper, with contribution from S.G., J.W., T.C. and JM.G. All authors have read and approved the manuscript.

REFERENCES

1. Megrian D, Taib N, Witwinowski J, Beloin C, Gribaldo S. 2020. One or two membranes? Diderm Firmicutes challenge the Gram-positive/Gram-negative divide. Mol Microbiol mmi.14469.

2. Veillon A, Zuber A. 1898. Recherches sur quelques microbes strictement anaérobies et leur rôle en pathologie humaine. Arch Med Exp Anat Pathol 10.

3. Dewhirst FE, Chen T, Izard J, Paster BJ, Tanner ACR, Yu W-H, Lakshmanan A, Wade WG. 2010. The human oral microbiome. J Bacteriol 192:5002–17.

4. van den Bogert B, Erkus O, Boekhorst J, de Goffau M, Smid EJ, Zoetendal EG, Kleerebezem M. 2013. Diversity of human small intestinal *Streptococcus* and *Veillonella* populations. FEMS Microbiol Ecol 85:376–388.

5. Aujoulat F, Roudière L, Picaud J-C, Jacquot A, Filleron A, Neveu D, Baum T-P, Marchandin H, Jumas-Bilak E. 2014. Temporal dynamics of the very premature infant gut dominant microbiota. BMC Microbiol 14:325.

6. Arrieta M-C, Stiemsma LT, Dimitriu PA, Thorson L, Russell S, Yurist-Doutsch S, Kuzeljevic B, Gold MJ, Britton HM, Lefebvre DL, Subbarao P, Mandhane P, Becker A, McNagny KM, Sears MR, Kollmann T, Investigators the CS, Mohn WW, Turvey SE, Finlay BB. 2015. Early infancy microbial and metabolic alterations affect risk of childhood asthma. Sci Transl Med 7:307ra152-307ra152.

7. Kolenbrander PE. 2011. Multispecies communities: Interspecies interactions influence growth on saliva as sole nutritional source, p. 49–54. *In* International Journal of Oral Science.

8. Periasamy S, Kolenbrander PE. 2010. Central role of the early colonizer Veillonella sp. in establishing multispecies biofilm communities with initial, middle, and late colonizers of enamel. J Bacteriol 192:2965–72.

9. Li J, Chen P, Li J, Gao X, Chen X, Chen J. 2017. A new treatment of sepsis caused by *veillonella parvula* : A case report and literature review. J Clin Pharm Ther 42:649–652.

10. Hirai J, Yamagishi Y, Kinjo T, Hagihara M, Sakanashi D, Suematsu H, Fujita J, Mikamo H. 2016. Osteomyelitis caused by Veillonella species: Case report and review of the literature. J Infect Chemother 22:417–420.

570 11. Gouze H, Noussair L, Padovano I, Salomon E, de Laroche M, Duran C, Felter A,
571 Carlier R, Breban M, Dinh A. 2019. Veillonella parvula spondylodiscitis. Médecine
572 Mal Infect 49:54–58.

573 12. Hyo Y, Fukushima H, Harada T, Hara H. 2019. Nasal septal abscess caused by
574 anaerobic bacteria of oral flora. Auris Nasus Larynx 46:147–150.

575 13. Wellens L, Casteels I, Huygens M. 2019. Veillonella parvula periorbital cellulitis: an
576 unusual pathogen causing a common clinical sign. GMS Ophthalmol cases 9:Doc17.

577 14. Gronow S, Welnitz S, Lapidus A, Nolan M, Ivanova N, del Rio TG, Copeland A, Chen
578 F, Tice H, Pitluck S, Cheng JF, Saunders E, Brettin T, Han C, Detter JC, Bruce D,
579 Goodwin L, Land M, Hauser L, Chang YJ, Jeffries CD, Pati A, Mavromatis K,
580 Mikhailova N, Chen A, Palaniappan K, Chain P, Rohde M, Göker M, Bristow J, Eisen
581 JA, Markowitz V, Hugenholtz P, Kyrpides NC, Klenk HP, Lucas S. 2010. Complete
582 genome sequence of Veillonella parvula type strain (Te3 T). Stand Genomic Sci 2:57–
583 65.

584 15. Poppleton DI, Duchateau M, Hourdel V, Matondo M, Flechsler J, Klingl A, Beloin C,
585 Gribaldo S. 2017. Outer membrane proteome of Veillonella parvula: A diderm
586 firmicute of the human microbiome. Front Microbiol 8:1–17.

587 16. Berne C, Ducret A, Hardy GG, Brun Y V. 2015. Adhesins Involved in Attachment to
588 Abiotic Surfaces by Gram-Negative Bacteria. Microbiol Spectr 3.

589 17. Knapp S, Brodal C, Peterson J, Qi F, Kreth J, Merritt J. 2017. Natural Competence Is
590 Common among Clinical Isolates of Veillonella parvula and Is Useful for Genetic
591 Manipulation of This Key Member of the Oral Microbiome. Front Cell Infect
592 Microbiol 7:1–12.

593 18. Branda SS, González-Pastor JE, Dervyn E, Ehrlich SD, Losick R, Kolter R. 2004.
594 Genes involved in formation of structured multicellular communities by Bacillus
595 subtilis. J Bacteriol 186:3970–9.

596 19. Dembek M, Barquist L, Boinett CJ, Cain AK, Mayho M, Lawley TD, Fairweather NF,
597 Fagan RP. 2015. High-Throughput Analysis of Gene Essentiality and Sporulation in
598 Clostridium difficile. MBio 6:e02383.

599 20. Łyskowski A, Leo JC, Goldman A. 2011. Structure and Biology of Trimeric
600 Autotransporter Adhesins, p. 143–158. *In* Advances in experimental medicine and

biology.

21. Ruiz-Ranwez V, Posadas DM, Estein SM, Abdian PL, Martin FA, Zorreguieta A. 2013. The BtaF trimeric autotransporter of Brucella suis is involved in attachment to various surfaces, resistance to serum and virulence. PLoS One 8:e79770.

22. Zhou P, Liu J, Merritt J, Qi F. 2015. A YadA-like autotransporter, Hag1 in Veillonella atypica is a multivalent hemagglutinin involved in adherence to oral streptococci, Porphyromonas gingivalis, and human oral buccal cells. Mol Oral Microbiol 30:269–279.

23. Trunk T, S. Khalil H, C. Leo J. 2018. Bacterial autoaggregation. AIMS Microbiol 4:140–164.

24. Bongrand C, Ruby EG. 2019. The impact of Vibrio fischeri strain variation on host colonization. Curr Opin Microbiol 50:15–19.

25. Bonazzi D, Lo Schiavo V, Machata S, Djafer-Cherif I, Nivoit P, Manriquez V, Tanimoto H, Husson J, Henry N, Chaté H, Voituriez R, Duménil G. 2018. Intermittent Pili-Mediated Forces Fluidize Neisseria meningitidis Aggregates Promoting Vascular Colonization. Cell 174:143-155.e16.

26. Klemm P, Vejborg RM, Sherlock O. 2006. Self-associating autotransporters, SAATs: Functional and structural similarities. Int J Med Microbiol 296:187–195.

27. Ageorges V, Schiavone M, Jubelin G, Caccia N, Ruiz P, Chafsey I, Bailly X, Dague E, Leroy S, Paxman J, Heras B, Chaucheyras-Durand F, Rossiter AE, Henderson IR, Desvaux M. 2019. Differential homotypic and heterotypic interactions of antigen 43 (Ag43) variants in autotransporter-mediated bacterial autoaggregation. Sci Rep 9:11100.

28. Wells TJ, Sherlock O, Rivas L, Mahajan A, Beatson SA, Torpdahl M, Webb RI, Allsopp LP, Gobius KS, Gally DL, Schembri MA. 2008. EhaA is a novel autotransporter protein of enterohemorrhagic Escherichia coli O157:H7 that contributes to adhesion and biofilm formation. Environ Microbiol 10:589–604.

29. Totsika M, Wells TJ, Beloin C, Valle J, Allsopp LP, King NP, Ghigo J-M, Schembri MA. 2012. Molecular characterization of the EhaG and UpaG trimeric autotransporter proteins from pathogenic Escherichia coli. Appl Environ Microbiol 78:2179–89.

30. Valle J, Mabbett AN, Ulett GC, Toledo-Arana A, Wecker K, Totsika M, Schembri

632 MA, Ghigo J-M, Beloin C. 2008. UpaG, a New Member of the Trimeric
633 Autotransporter Family of Adhesins in Uropathogenic Escherichia coli. J Bacteriol
634 190:4147–4161.

635 31. Paton AW, Srimanote P, Woodrow MC, Paton JC. 2001. Characterization of Saa, a
636 novel autoagglutinating adhesin produced by locus of enterocyte effacement-negative
637 Shiga-toxigenic Escherichia coli strains that are virulent for humans. Infect Immun
638 69:6999–7009.

639 32. Leo JC, Lyskowski A, Hattula K, Hartmann MD, Schwarz H, Butcher SJ, Linke D,
640 Lupas AN, Goldman A. 2011. The Structure of E. coli IgG-Binding Protein D Suggests
641 a General Model for Bending and Binding in Trimeric Autotransporter Adhesins.
642 Structure 19:1021–1030.

643 33. Beloin C, Michaelis K, Lindner K, Landini P, Hacker J, Ghigo J-M, Dobrindt U. 2006.
644 The transcriptional antiterminator RfaH represses biofilm formation in Escherichia
645 coli. J Bacteriol 188:1316–31.

646 34. Korea C-G, Badouraly R, Prevost M-C, Ghigo J-M, Beloin C. 2010. Escherichia coli
647 K-12 possesses multiple cryptic but functional chaperone-usher fimbriae with distinct
648 surface specificities. Environ Microbiol 12:1957–1977.

649 35. Hasman H, Chakraborty T, Klemm P. 1999. Antigen-43-mediated autoaggregation of
650 Escherichia coli is blocked by fimbriation. J Bacteriol 181:4834–41.

651 36. Schembri MA, Dalsgaard D, Klemm P. 2004. Capsule shields the function of short
652 bacterial adhesins. J Bacteriol 186:1249–57.

653 37. Hughes C V, Andersen RN, Kolenbrander PE. 1992. Characterization of Veillonella
654 atypica PK1910 adhesin-mediated coaggregation with oral Streptococcus spp. Infect
655 Immun 60:1178–86.

656 38. Mashima I, Nakazawa F. 2015. Interaction between Streptococcus spp. and Veillonella
657 tobetsuensis in the early stages of oral biofilm formation. J Bacteriol. American Society
658 for Microbiology.

659 39. Mashima I, Nakazawa F. 2014. The influence of oral Veillonella species on biofilms
660 formed by Streptococcus species. Anaerobe 28:54–61.

661 40. Periasamy S, Kolenbrander PE. 2010. Central role of the early colonizer Veillonella sp.
662 in establishing multispecies biofilm communities with initial, middle, and late

colonizers of enamel. J Bacteriol 192:2965–2972.

41. Hughes C V, Kolenbrander PE, Andersen RN, Moore L V. 1988. Coaggregation properties of human oral Veillonella spp.: relationship to colonization site and oral ecology. Appl Environ Microbiol 54:1957–63.

42. Wells TJ, Totsika M, Schembri MA. 2010. Autotransporters of Escherichia coli: A sequence-based characterization. Microbiology 156:2459–2469.

43. El-Gebali S, Mistry J, Bateman A, Eddy SR, Luciani A, Potter SC, Qureshi M, Richardson LJ, Salazar GA, Smart A, Sonnhammer ELL, Hirsh L, Paladin L, Piovesan D, Tosatto SCE, Finn RD. 2019. The Pfam protein families database in 2019. Nucleic Acids Res 47.

44. Mesnage S, Fontaine T, Mignot T, Delepierre M, Mock M, Fouet A. 2000. Bacterial SLH domain proteins are non-covalently anchored to the cell surface via a conserved mechanism involving wall polysaccharide pyruvylation. EMBO J 19:4473–4484.

45. Park JS, Lee WC, Yeo KJ, Ryu K-S, Kumarasiri M, Hesek D, Lee M, Mobashery S, Song JH, Kim S Il, Lee JC, Cheong C, Jeon YH, Kim H-Y. 2012. Mechanism of anchoring of OmpA protein to the cell wall peptidoglycan of the gram-negative bacterial outer membrane. FASEB J 26:219–228.

46. Minazzato G, Gasparrini M, Amici A, Cianci M, Mazzola F, Orsomando G, Sorci L, Raffaelli N. 2020. Functional characterization of COG1713 (YqeK) as a novel diadenosine tetraphosphate hydrolase family. J Bacteriol JB.00053-20.

47. Monds RD, Newell PD, Wagner JC, Schwartzman JA, Lu W, Rabinowitz JD, O'Toole GA. 2010. Di-adenosine tetraphosphate (Ap4A) metabolism impacts biofilm formation by Pseudomonas fluorescens via modulation of c-di-GMP-dependent pathways. J Bacteriol 192:3011–3023.

48. Gundlach J, Rath H, Herzberg C, Mäder U, Stülke J. 2016. Second Messenger Signaling in Bacillus subtilis: Accumulation of Cyclic di-AMP Inhibits Biofilm Formation. Front Microbiol 7:804.

49. Peng X, Zhang Y, Bai G, Zhou X, Wu H. 2016. Cyclic di-AMP mediates biofilm formation. Mol Microbiol 99:945–959.

50. Townsley L, Yannarell SM, Huynh TN, Woodward JJ, Shank EA. 2018. Cyclic di-AMP Acts as an Extracellular Signal That Impacts Bacillus subtilis Biofilm Formation

694 and Plant Attachment. MBio 9.

695 51. Jenal U, Reinders A, Lori C. 2017. Cyclic di-GMP: second messenger extraordinaire.
696 Nat Rev Microbiol 15:271–284.

697 52. Krasteva PV, Sondermann H. 2017. Versatile modes of cellular regulation via cyclic
698 dinucleotides. Nat Chem Biol 13:350–359.

699 53. Yan F, Yu Y, Wang L, Luo Y, Guo J-H, Chai Y. 2016. The comER Gene Plays an
700 Important Role in Biofilm Formation and Sporulation in both Bacillus subtilis and
701 Bacillus cereus. Front Microbiol 7:1025.

702 54. Koren S, Walenz BP, Berlin K, Miller JR, Bergman NH, Phillippy AM. 2017. Canu:
703 scalable and accurate long-read assembly via adaptive k-mer weighting and repeat
704 separation. Genome Res 27:722–736.

705 55. Walker BJ, Abeel T, Shea T, Priest M, Abouelliel A, Sakthikumar S, Cuomo CA, Zeng
706 Q, Wortman J, Young SK, Earl AM. 2014. Pilon: An Integrated Tool for
707 Comprehensive Microbial Variant Detection and Genome Assembly Improvement.
708 PLoS One 9:e112963.

709 56. Cokelaer T, Desvillechabrol D, Legendre R, Cardon M, Cokelaer T, Desvillechabrol D,
710 Legendre R, Cardon M. 2017. “Sequana”: a Set of Snakemake NGS pipelines. J Open
711 Source Softw 2:352.

712 57. Desvillechabrol D, Bouchier C, Kennedy S, Cokelaer T. 2018. Sequana Coverage:
713 Detection and Characterization of Genomic Variations using Running Median and
714 Mixture Models. Gigascience 7.

715 58. Simão FA, Waterhouse RM, Ioannidis P, Kriventseva E V., Zdobnov EM. 2015.
716 BUSCO: assessing genome assembly and annotation completeness with single-copy
717 orthologs. Bioinformatics 31:3210–3212.

718 59. Seemann T. 2014. Prokka: rapid prokaryotic genome annotation. Bioinformatics
719 30:2068–2069.

720 60. Johnson LS, Eddy SR, Portugaly E. 2010. Hidden Markov model speed heuristic and
721 iterative HMM search procedure. BMC Bioinformatics 11:431.

722 61. Lupas A, Dyke M Van, Stock J. 1991. Predicting Coiled Coils from Protein Sequences.
723 Science (80-). American Association for the Advancement of Science.

62. Abby SS, Néron B, Ménager H, Touchon M, Rocha EPC. 2014. MacSyFinder: A Program to Mine Genomes for Molecular Systems with an Application to CRISPR-Cas Systems. PLoS One 9:e110726.

63. Letunic I, Bork P. 2019. Interactive Tree Of Life (iTOL) v4: recent updates and new developments. Nucleic Acids Res 47:W256–W259.

64. Fagan RP, Fairweather NF. 2011. *Clostridium difficile* Has Two Parallel and Essential Sec Secretion Systems. J Biol Chem 286:27483–27493.

65. Ghigo J-M. 2001. Natural conjugative plasmids induce bacterial biofilm development. Nature 412:442–445.

66. Beloin C, Valle J, Latour-Lambert P, Faure P, Kzreminski M, Balestrino D, Haagensen JAJ, Molin S, Prensier G, Arbeille B, Ghigo J-M. 2003. Global impact of mature biofilm lifestyle on Escherichia coli K-12 gene expression. Mol Microbiol 51:659–674.

67. Soutourina OA, Monot M, Boudry P, Saujet L, Pichon C, Sismeiro O, Semenova E, Severinov K, Le Bouguenec C, Coppée JY, Dupuy B, Martin-Verstraete I. 2013. Genome-Wide Identification of Regulatory RNAs in the Human Pathogen Clostridium difficile. PLoS Genet 9.

68. Liu J, Xie Z, Merritt J, Qi F. 2012. Establishment of a tractable genetic transformation system in Veillonella spp. Appl Environ Microbiol 78:3488–91.

69. Sullivan MJ, Petty NK, Beatson SA. 2011. Easyfig: a genome comparison visualizer. Bioinformatics 27:1009–1010.

746 **TABLES**

747

748

Locus tag	PROKKA Gene name	Genome position		Gene size (kb)	Strand	Description	DSM2008 homolog	Name	Class
FNLLGLLA_00032	prn 1	39,354	41,723	2,37	forward	Autotransporter	fusion Vpar_0036-0037	VmaA	Va
FNLLGLLA_00034	btaE 1	42,345	43,754	1,41	reverse	Trimeric Autotransporter: YadA like	Vpar_0039	VtaB	Vc
FNLLGLLA_00035	hypothetical protein	44,146	45,189	1,04	forward	Autotransporter (partial)	Vpar_0040		Ve
FNLLGLLA_00036	hypothetical protein	45,453	46,883	1,431	forward	none	split Vpar_0041		?
FNLLGLLA_00037	omp-alpha	46,91	47,878	969	forward	Trimeric Autotransporter/ S-layer homology domain	split Vpar_0041		Vc?
FNLLGLLA_00038	upaG 1	48,397	56,829	8,433	forward	Trimeric Autotransporter: YadA like	Vpar_0042	VtaC	Vc
FNLLGLLA_00040	btaE 2	57,966	59,84	1,875	forward	Trimeric Autotransporter: YadA like (Partial)	split Vpar_0048		?
FNLLGLLA_00041	ata 1	59,837	63,463	3,627	forward	Trimeric Autotransporter: YadA like	split Vpar_0048		Vc?
FNLLGLLA_00044	ehaG 1	65,3	71,515	6,216	forward	Trimeric Autotransporter: YadA like	Vpar_0051	VtaD	Vc
FNLLGLLA_00045	upaG 2	71,995	81,42	9,426	forward	Trimeric Autotransporter: YadA like	Vpar_0052	VtaE	Vc
FNLLGLLA_00046	ata 2	81,941	91,519	9,579	forward	Trimeric Autotransporter: YadA like	Vpar_0053	VtaF	Vc
FNLLGLLA_00098	btaE 3	151,792	153,522	1,731	forward	Trimeric Autotransporter/ S-layer homology domain	Vpar_0100	VtaG	Vc
FNLLGLLA_00099	ata 3	154,024	158,982	4,959	forward	Trimeric Autotransporter/ S-layer homology domain	absent	VtaH	Vc
FNLLGLLA_00335	prn 2	414,666	416,888	2,223	forward	Autotransporter	Vpar_0330	VmaB	Va
FNLLGLLA_00516	btaF	581,236	590,358	9,123	forward	Trimeric Autotransporter: YadA like	Vpar_0464	VtaA	Vc
FNLLGLLA_00581	brkA	668,34	670,583	2,244	forward	Autotransporter	Vpar_1322	VmaC	Va
FNLLGLLA_01790	ehaG 2	1,943,661	1,946,159	2,499	reverse	Trimeric Autotransporter/ S-layer homology domain	Vpar_1664	VtaI	Vc

749 Table 1 : ***V. parvula*** **SKV38 autotransporters**

750

Strain name	Description	Reference
WT	*Veillonella parvula* SKV38	(17)
9G5	*Veillonella parvula* SKV38 *FNLLGLLA_00516::Transposon*	This study
5C5	*Veillonella parvula* SKV38 *FNLLGLLA_00516::Transposon*	This study
5H1	*Veillonella parvula* SKV38 *FNLLGLLA_00516::Transposon*	This study
3D6	*Veillonella parvula* SKV38 *FNLLGLLA_00516::Transposon*	This study
7B11	*Veillonella parvula* SKV38 *FNLLGLLA_00516::Transposon*	This study
2F7	*Veillonella parvula* SKV38 *FNLLGLLA_00516::Transposon*	This study
3F7	*Veillonella parvula* SKV38 *FNLLGLLA_00516::Transposon*	This study
5E11	*Veillonella parvula* SKV38 *FNLLGLLA_01127::Transposon*	This study
ΔvtaA	*Veillonella parvula* SKV38 Δ*FNLLGLLA_00516::tetM*	This study
pTet-vtaA	*Veillonella parvula* SKV38 *catP-Term(fdx)-Ptet-FNLLGLLA_00516*	This study
Δ8	*Veillonella parvula* SKV38 Δ*FNLLGLLA_00036-46::tetM*	This study
ΔvmaA	*Veillonella parvula* SKV38 Δ*FNLLGLLA_00032::tetM*	This study
ΔvtaB	*Veillonella parvula* SKV38 Δ*FNLLGLLA_00034::tetM*	This study
ΔvtaG	*Veillonella parvula* SKV38 Δ*FNLLGLLA_00098::tetM*	This study
ΔvtaH	*Veillonella parvula* SKV38 Δ*FNLLGLLA_00099::tetM*	This study
ΔvmaB	*Veillonella parvula* SKV38 Δ*FNLLGLLA_00335::tetM*	This study
ΔvmaC	*Veillonella parvula* SKV38 Δ*FNLLGLLA_00581::tetM*	This study
ΔvtaI	*Veillonella parvula* SKV38 Δ*FNLLGLLA_01790::tetM*	This study
ΔvtaAΔ8	*Veillonella parvula* SKV38 Δ*FNLLGLLA_ 00516::catP* Δ*FNLLGLLA_00036-46::tetM*	This study
Δ1127	*Veillonella parvula* SKV38 Δ*FNLLGLLA_01127::tetM*	This study
Δ1127Δ8	*Veillonella parvula* SKV38 Δ*FNLLGLLA_01127::tetM* Δ*FNLLGLLA_00036-46::catP*	This study
WT+pEmpty	*Veillonella parvula* SKV38-pBSJL2-*catP-pmdh*	This study
Δ1127+pEmpty	*Veillonella parvula* SKV38 ΔFNLLGLLA_01127::*tetM*-pBSJL2-*catP-pmdh*	This study
Δ1127+p1127	*Veillonella parvula* SKV38 ΔFNLLGLLA_01127::*tetM*-pBSJL2-*catP-pmdh-FNLLGLLA_01127*	This study
P_{tet}-φ	SKV38- pRPF185*ΔgusA*	This study
P_{tet}-*gusA*	SKV38- pRPF185	This study
P_{Cwp2} -*gusA*	SKV38- pRPF144	This study

Plasmid	Description	Reference

pRPF215	*mariner* Tn delivery plasmid, P_{tet}::*Himar1*, ITR-*ermB*-ITR, *catP*, *tetR*	(19)
pRPF185	tetracycline inducible expression system fused with ß-glucuronidase *gusA* Term(fdx)- P_{tet} -gusA-Term(slpA), *catP*	(64)
pRPF185Δ*gusA*	pDIA6103, tetracycline inducible expression system Term(fdx)-P_{tet}-Term(slpA), *catP*	(67)
pRPF144	*carries a Clostridium* constitutitive promoter fused with *gusA* P_{Cwp2}-*gusA*	(64)
pBSJL2	*E. coli-Veillonella* shuttle plasmid, P_{gyrA}::*tetM*	(68)
pBSJL2-cat	*E. coli-Veillonella* shuttle plasmid, P_{cat}::*catP*, *pmdh* promoter	This study
p1127	pBSJL2-*catP-pmdh-FNLLGLLA_01127*	This study

751 **Table 2: Strains and plasmids used in this study**

752

753

754

FIGURES LEGEND

Figure 1: **Random transposon mutagenesis in *Veillonella parvula* SKV38 led to identification of mutants with reduced biofilm formation. A**. 96-well polystyrene plate biofilm assay after CV staining of nine transposon mutants identified by random mutagenesis grown 24h in BHILC. Mean of WT is adjusted to 100 %. Min-max boxplot of 6-15 biological replicates for each strain are represented, each replicate is the mean of two technical replicates. * p-value<0.05, ** p-value <0.005, Mann-Whitney test. **B**. Schematic representation of the transposon insertion point identified (red arrow) for the 8 transposon mutants. Blue bar represents the size of the gene in nucleotides.

Figure 2: **VtaA is an adhesin involved in auto-aggregation and biofilm formation**. **A**. 96-well plate biofilm assay after 24h growth in BHILC. Mean of WT is adjusted to 100 %. Min-max boxplot of 6 biological replicates for each strain. * p-value<0.05, ** p-value <0.005, Mann-Whitney test between strains. **B.** and **C.** Aggregation curve in spectrophotometry cuvette of WT and Δ*vtaA* (**B**) and of an inducible *vtaA* with 0, 0.025 or 0.1 µg/mL of the inducer aTc (**C**). 100 % represent lack of aggregation, 0 % complete sedimentation of the culture. Median of 6 biological replicates, error bars represent 95% confidence interval. At each time points we computed the Mann-Whitney test between conditions. We applied Bonferroni correction for multiple testing: p-value are only considered significant if *p-value<0.004, **p-value<0.0004, ***p-value<0.00004. Indicated p-values were calculated by comparing in **B,** WT and Δ*vtaA*, and in **C**, *pTet-vtaA* without aTc and *pTet-vtaA* with different aTc concentrations. **D**. 96-well plate biofilm assay after 24h growth of an inducible *vtaA* in BHILC with different concentrations of aTc. WT without aTc is adjusted to 100 %. Median of 6 biological replicates, each replicate corresponds to the mean of two technical replicates, error bars represent 95% confidence interval. * p-value<0.05, ** p-value <0.005, Mann-Whitney test. **E**. Biofilm formation in continuous flow microfermentor on glass spatula during 48h in BHILC. WT was adjusted to 100 %. Min-max boxplot of 4 biological replicates for each strain. A picture of the spatula before resuspension is shown below each boxplot bar. * p-value<0.05, Mann-Whitney test.

Figure 3: ***Veillonella parvula* autotransporters domain organization. A.** Genetic organization of the *V. parvula* SKV38 autotransporter adhesin gene cluster and the corresponding adhesin domain organization. **B**. Domain organization of the six remaining *V. parvula* SKV38 autotransporter adhesins encoded by genes located outside of the cluster. Domains were detected with the HMMER package (60), only the domains with e-values lower than 10^{-3} are shown. Presence of C-terminal coils structure was determined using the COILS program (https://embnet.vital-it.ch/software/COILS_form.html). All *V. parvula* trimeric ATs display an additional C-terminal domain (a SLH or a coiled coil domain) following the YadA anchor domain as compared to classical trimeric autotransporters.

Figure 4: **Synteny of the adhesin gene cluster in a selection of *Veillonella* species**. The synteny of the proteins of the cluster between the closest relatives was assessed using EasyFig (69). Oblique lines between genes represent tblastx identities (program parameters: maximum e-value of 10^{12}, minimum length of 30, minimum identity of 30). The *V. parvula* SKV38 strain

used in this study is presented in red. The annotation of the genes of the cluster is indicated on the right.

Figure 5: **A cluster of eight trimeric autotransporters is involved in surface binding. A.** Aggregation curve in spectrophotometry cuvette. 100 % represent lack of aggregation, 0 % complete sedimentation of the culture. Median of 6 biological replicates, error bars represent 95% confidence interval. * Mann-Whitney test, corrected for multiple testing with Bonferroni correction: significance is achieved if p-value < 0.007. **B.** and **C.** 96-well plate biofilm assay after 24 h growth in BHILC. Mean of WT is adjusted to 100 %. Min-max boxplot of 6 biological replicates for each strain, each replicate is the mean of two technical replicates. In **B.** we applied a Mann-Whitney; * p-value<0.05, ** p-value <0.005. In **C.** we applied Bonferroni correction for multiple testing: tests were called significant only if p-value<0.01: * p-value<0.01, ** p-value <0.001, *** p-value <0.0001. **D.** Biofilm formation in continuous flow microfermentor on glass spatula during 48h in BHILC. WT was adjusted to 100 %. Min-max boxplot of 4 biological replicates for each strain. * p-value<0.05, Mann-Whitney test. A picture of spatula before resuspension is shown for each mutant below the boxplot. **E.** Initial adhesion on glass spatula. Percentage of CFU that adhered to the spatula controlled by the number of CFU of the inoculation solution. Min-max boxplot of 6-9 replicates per strain is represented. * p-value<0.05, ** p-value <0.005, *** p-value <0.0005, Mann-Whitney test.

Figure 6**: Occurrence and synteny of HD Phosphatase (YqeK) in diderm and monoderm bacteria**. **A.** The presence of the cluster was investigated using MacSyFinder (62) and the results were plotted onto a schematic reference tree of 187 cultivable bacteria among the 390 of the analyzed databank. The cell wall status of each phylum is indicated as: (-) diderm with LPS, (+) monoderm, (atyp.) diderm without LPS, (?) unclear. For the Firmicutes, the diderm lineages are indicated in red (Negativicutes), blue (Halanaerobiales) and purple (Limnochordales).

Figure 7: **FNLLGLLA_01127 represses biofilm formation in microfermentor**. **A.** 96-well plate biofilm assay after 24 h growth in BHLC corrected by OD_{600} after 24 h growth in plate. Mean of WT is adjusted to 100 %. Min-max boxplot of 6 biological replicates for each strain, each replicate is the mean of two technical replicates. * p-value < 0.05, Mann-Whitney test. **B.** Aggregation curve in spectrophotometry cuvette. 100 % represent lack of aggregation, 0 % complete sedimentation of the culture. Median of 6 biological replicates, error bars represent 95% confidence interval. * Mann-Whitney test, corrected for multiple testing with Bonferroni correction: significance is achieved if p-value<0.007. **C.** Biofilm formation in continuous flow microfermentor on glass spatula during 48h in BHILC. Mean of WT is adjusted to 100 %. Min-max boxplot of 4 biological replicates for each strain. * p-value < 0.05, ** p-value<0.005, Mann-Whitney test. A picture of a spatula before resuspension is shown for each strain below the histogram. **D.** Biofilm formation in continuous flow microfermentor on glass spatula during 48h in BHILC+chloramphenicol. Mean of WT+pEmpty is adjusted to 100 %. Min-max boxplot of 4 biological replicates for each strain. * p-value < 0.05, Mann-Whitney test. A picture of a spatula before resuspension is shown for each strain below the boxplot. **E.** Scanning electronic microscopy of Δ1127 biofilm grown under continuous flow of BHILC in microfermentor on a plastic microscopy slide. Magnification 2K and 5K. **F.** Initial adhesion on glass spatula. Percentage of CFU that adhered to the spatula in 30 min controlled by the number of CFU of

the inoculation solution. Min-max boxplot of 6-9 replicates per strain. * p-value<0.05, Mann-Whitney test.

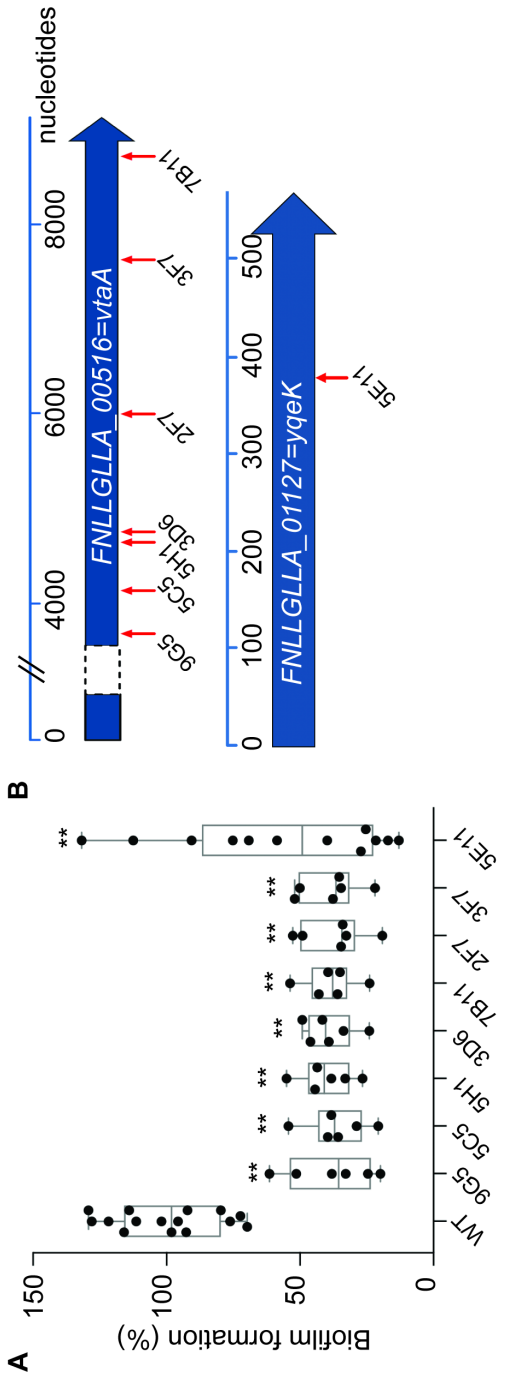

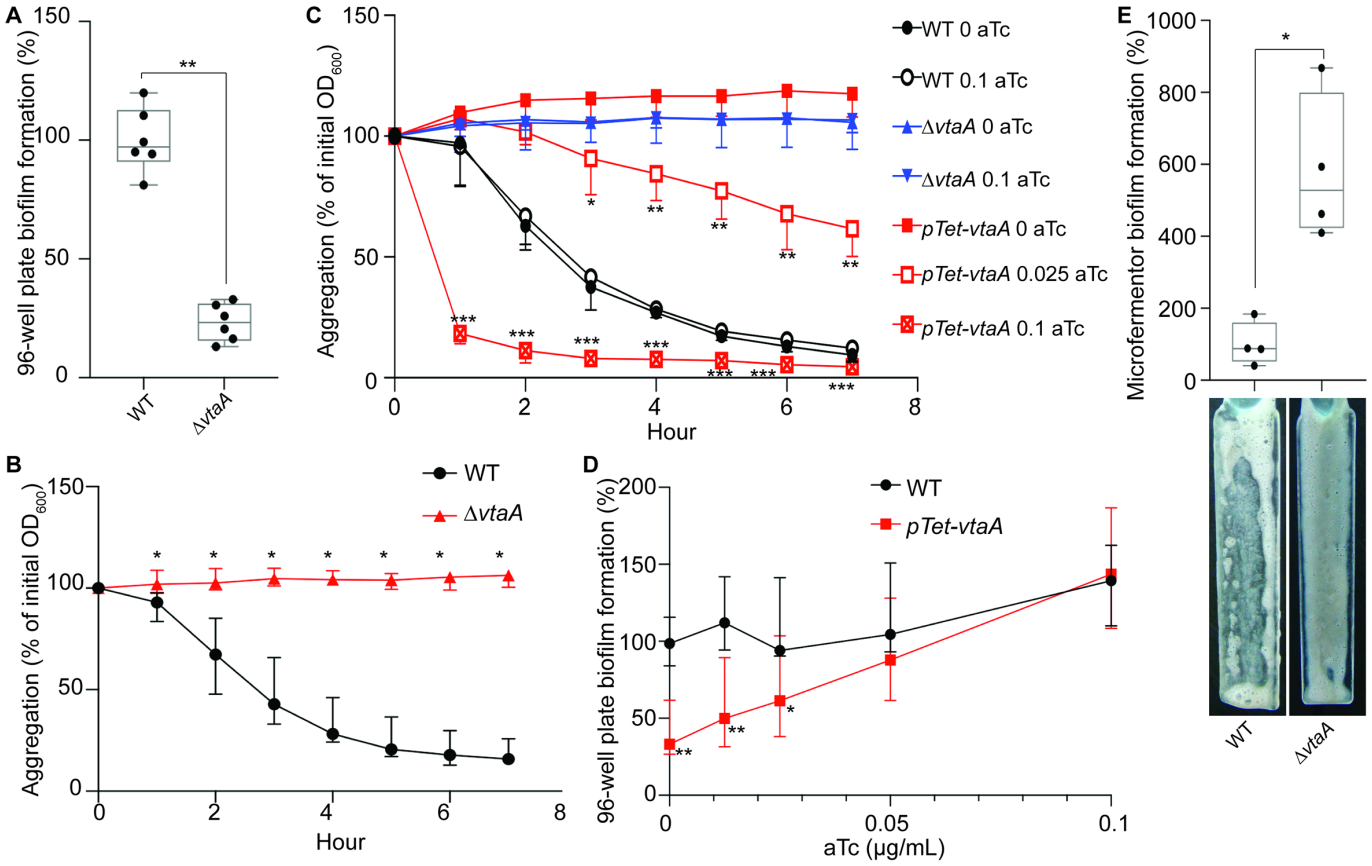

A

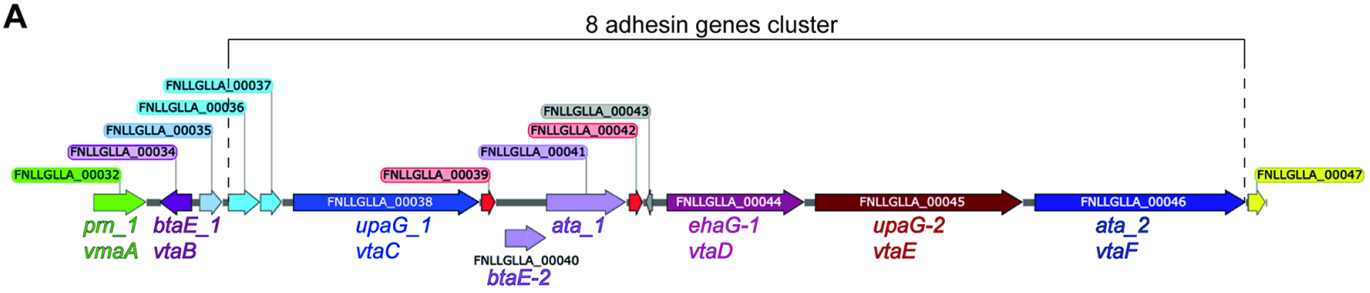

Gene locus	Protein name	Domain organization
FNLLGLLA_00032	Prn_1 / VmaA	790 aa
FNLLGLLA_00034	BtaE_1 / VtaB	470 aa
FNLLGLLA_00035		348 aa
FNLLGLLA_00036		477 aa
FNLLGLLA_00037		323 aa
FNLLGLLA_00038	UpaG_1 / VtaC	2811 aa
FNLLGLLA_00040	BtaE_2	625 aa
FNLLGLLA_00041	Ata_1	1209 aa
FNLLGLLA_00044	EhaG_1 / VtaD	2072 aa
FNLLGLLA_00045	UpaG_2 / VtaE	3142 aa
FNLLGLLA_00046	Ata_2 / VtaF	3193 aa

B

Gene locus	Protein name	Domain organization
FNLLGLLA_00098	BtaE_3 / VtaG	577 aa
FNLLGLLA_00099	Ata_3 / VtaH	1653 aa
FNLLGLLA_00335	Prn_2 / VmaB	741 aa
FNLLGLLA_00516	BtaF / VtaA	3041 aa
FNLLGLLA_00581	BrkA / VmaC	748 aa
FNLLGLLA_01790	EhaG_2 / VtaI	833 aa

1000 aa

- extended signal peptide region (PF13018)
- procyclic acidic repetitive protein (PF05887)
- DUF1664 (PF07889)
- YadA head (PF05658)
- YadA stalk (PF05662)
- autotransporter (PF03797)
- inverse autotransporter beta domain (PF11924)
- YadA anchor (PF03895)
- S-layer homology (PF00395)
- Coil (Coils prediction)